energies

MDPI

Article

Experimental Research on the Flow and Heat Transfer Characteristics of Subcritical and Supercritical Water in the Vertical Upward Smooth and Rifled Tubes

Xiaocheng Du, Weiteng Li, Xirong Zhang, Jingrong Chen, Tingyu Chen and Dong Yang *

State Key Laboratory of Multiphase Flow in Power Engineering, Xi'an Jiaotong University, Xi'an 710049, China
* Correspondence: dyang@mail.xjtu.edu.cn

Abstract: Experiments were conducted to investigate the heat transfer and flow characteristics of the vertical upward smooth and rifled tubes from subcritical to supercritical pressure. The distributions of wall temperature and heat transfer coefficient (HTC) were obtained, and the HTC correlations and friction resistance coefficient correlations were fitted with experimental data. In addition, the influences of heat flux and type of tube on heat transfer performance were analyzed. The research shows that heat flux has different influences on the heat transfer characteristics under different pressures. The increase in heat flux improves the heat transfer characteristics in the nucleate boiling region, yet it leads to the advance in heat transfer deterioration. However, for supercritical water, the increase in heat flux reduces the heat transfer ability. In addition, using the rifled tube not only improves the heat transfer performance, but also inhibits the occurrence of heat transfer deterioration. The fitted correlations have great predictive ability for the heat transfer coefficient and friction resistance coefficient, and the average relative fitting errors are limited to 20%.

Keywords: variable pressure operation; heat transfer coefficient; friction resistance coefficient; supercritical water; supercritical boiler

Citation: Du, X.; Li, W.; Zhang, X.; Chen, J.; Chen, T.; Yang, D. Experimental Research on the Flow and Heat Transfer Characteristics of Subcritical and Supercritical Water in the Vertical Upward Smooth and Rifled Tubes. *Energies* **2022**, *15*, 7941. https://doi.org/10.3390/en15217941

Academic Editors: Rafał Kobyłecki, Artur Blaszczuk, Xiaofeng Lu and Dongfang Li

Received: 25 August 2022
Accepted: 23 September 2022
Published: 26 October 2022

1. Introduction

Supercritical thermal power units usually adopt variable pressure operation. Generally, the units operate at stable pressure when they run above 85% load or below 35% load, and they operate at variable pressure when they run a load between 35 and 85%. This operation method makes the unit keep a stable pressure under a high load, which improves the cycle's efficiencies and the load-control ability. Units work with variable pressure under the middle load conditions, which ensures the stabilities of the volume flow rate in the steam turbine's blading components and temperature in the steam turbine's high-pressure cylinder. The operation with stable pressure can prevent flow instability under a low load. Therefore, variable pressure operation has not only a high cycle efficiency but also the advantage of rapid adjustment. Therefore, supercritical variable pressure operation has attracted increasing attention from researchers.

In order to improve the efficiency and control level, the premise is to grasp the heat transfer characteristics of the water wall. The typical process of pressure change with a supercritical thermal power unit load is shown in Figure 1. It can be seen that the water wall inlet pressure varies from subcritical pressure to supercritical pressure, and the phase of water varies between a single phase and the gas–liquid phase. This change complicates the flow and heat transfer characteristics of water and may result in flow instability or heat transfer deterioration [1,2]. Therefore, a comprehensive understanding of flow and heat transfer characteristics, such as heat transfer coefficient, critical heat flux, and critical enthalpy, can provide the theory and technology supports for developing supercritical thermal power units [3,4].

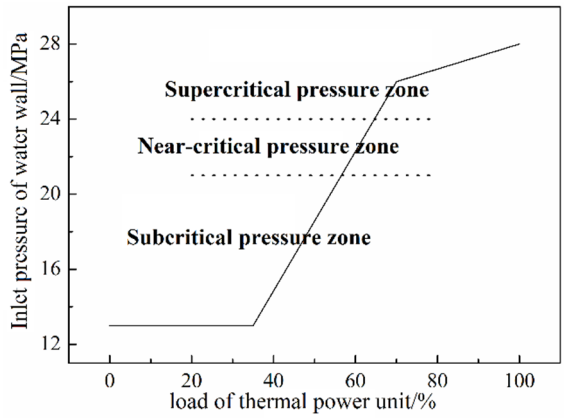

Figure 1. The relationship between water wall inlet pressure and supercritical thermal power unit load.

There are several studies on flow and heat transfer characteristics in supercritical boilers. Swenson et al. have found that the heat transfer coefficient has a peak near the pseudo-critical temperature, and the peak value decreases with the increase in the pressure and heat flux [5]. Vikhrev et al. have discovered that heat transfer deterioration (HTD) has two types [6]. One type is induced by the inlet effect of the test section that occurs at low mass flux and high heat flux conditions. Another type usually occurs when the wall temperature is higher than the pseudo-critical temperature. Yamagata et al. have found that the peak value of HTC always occurs in the location where the bulk temperature is below the pseudo-critical temperature and the inner wall temperature is greater than the pseudo-critical temperature [7]. In addition, they consider that the occurrence of HTD is determined by the ratio of heat flux to mass flux. Kolher et al. have analyzed the influence of the design of a rifled tube on the heat transfer performance [8]. Kafengaus has analyzed the experimental data of many fluids and proposed 'pseudo boiling' [9]. He considers 'pseudo boiling' to be induced by the phenomenon that low-density fluid near the inner wall flows into the tube center. Grabezhnaya et al. evaluated the typical heat transfer correlations and discovered that the correlations proposed by Bishop and Swenson were more suitable for heat transfer calculation [10]. Yoshida et al. have researched the influence of abrupt property variation on heat transfer at a supercritical pressure and discovered that the variation in the property will promote heat transfer [11]. Mokry et al. have collected many experimental data on supercritical water heat transfer and fitted a new correlation for heat transfer calculation [12].

For variable pressure operation, the pressure varies from subcritical pressure to supercritical pressure in supercritical thermal power unit. Therefore, it is vital to investigate the heat transfer and flow characteristics in a large pressure range. Although there are many experimental studies on the flow and heat transfer characteristics of supercritical water, there are few experimental parameters for the actual application of supercritical boilers. Experiments were conducted to obtain the exact experimental data for industrial applications. In addition, the application of rifled tubes for water-cooled walls are increasing. Experimental data for rifled tubes are also important, so the experiments for a rifled tube were also conducted. Finally, comprehensive heat transfer characteristics have been acquired based on the experimental results, which include heat transfer correlation, pressure drop, and heat transfer deterioration.

2. Experimental Setup and Data Processing

2.1. Experimental Setup

Figure 2 shows the flow chart of the experimental system. A detailed description can be found in our previous work [13,14]. Test sections with $\Phi 31.8 \times 5.5$ mm and 2000 mm height were made by SA-213T12. The designs of the smooth tube and the four-head ribbed tube are similar and are displayed in Figure 3. The equivalent diameter of the rifled tube is 19.75

mm. The structure of the rifled tube is listed in Table 1 and is shown in Figure 4. The outer wall temperatures were measured by 26 Φ0.2 mm K-type thermocouples, and the water temperatures were measured by Φ3 mm K-type thermocouples. The data for heat transfer characteristics were gathered in the test section, and the data for flow resistance were gathered in the horizontal resistance section because the effect of gravity was eliminated. The photo of the test section is shown in Figure 5.

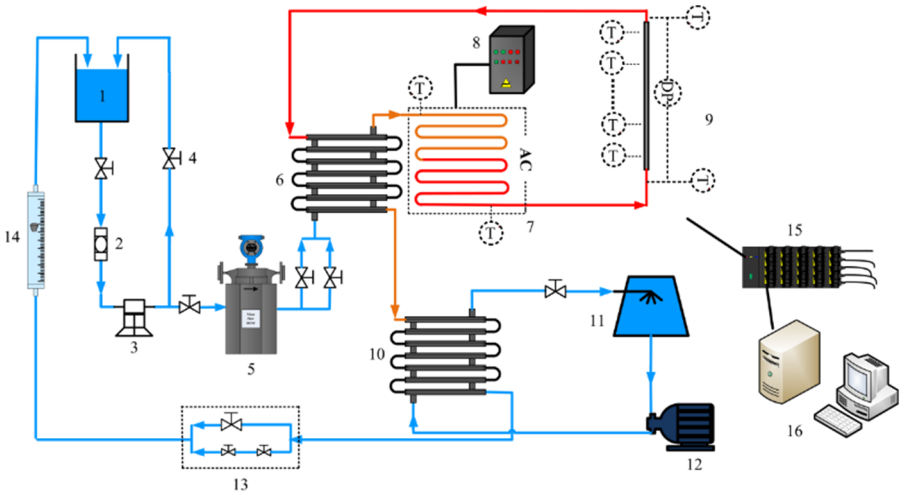

Figure 2. The flow chart of the experimental system.

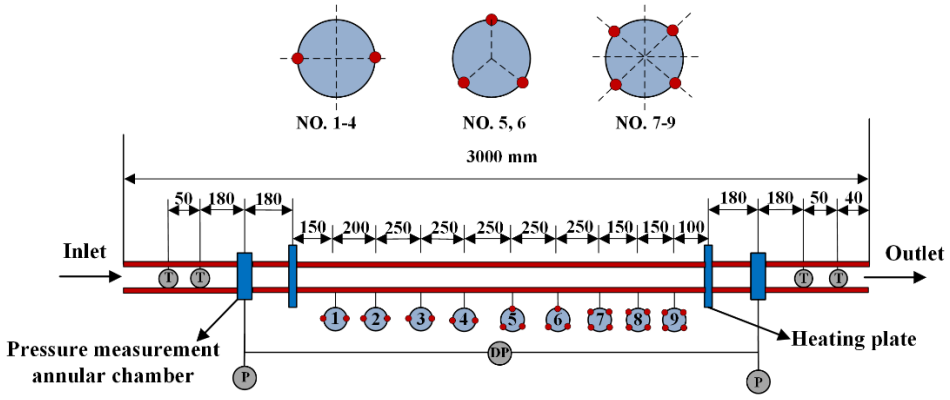

Figure 3. The design of the test section and the horizontal resistance section.

Table 1. The structural parameters of the rifled tube.

Parameter	Dimension
Outer diameter, d_{out}	31.8 mm
Maximum inner diameter, d_{max}	20.8 mm
Minimum inner diameter, d_{min}	18.1 mm
Hydraulic diameter, d_h	19.75 mm
Number of thread, N	4
Thread form	orthogon
Thread height, H	1.35 mm
Thread width, b	6 mm
Thread angle, a	43.6°
Pitch, S	17.5 mm

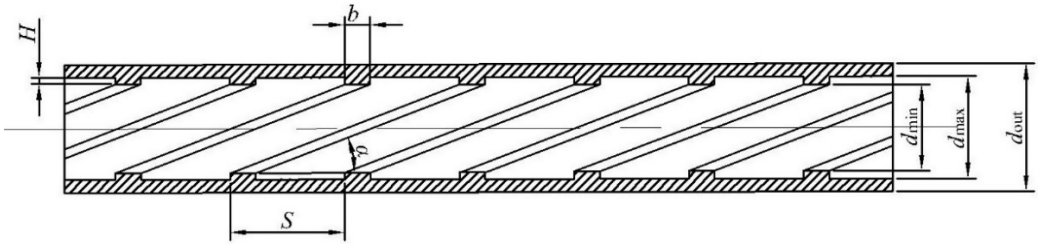

Figure 4. Structure of the four-head ribbed tube.

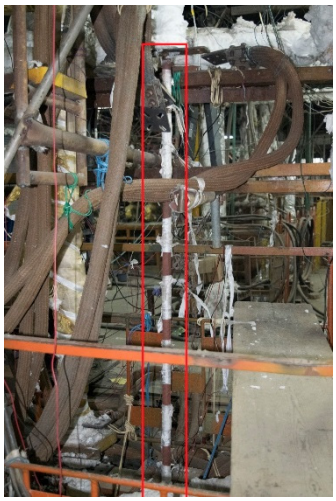

Figure 5. The photo of the test section.

Aiming at the variable pressure operation, experiments under different pressure conditions were conducted. The operating parameters are shown in Table 2. For the supercritical pressure, if the end enthalpy did not reach 2950 kJ/kg when the heat transfer deterioration occurred, then the end enthalpy could be changed to 2800 kJ/kg. The pressure, heat flux, and mass flux were fixed in every case. In order to cover the enthalpy range, the inlet temperature is raised by increasing the power of preheating section.

Table 2. The operating parameters of the experiments.

Case	Pressure MPa	Heat Flux kW/m^2	Mass Flux kg/(m^2·s)	Start Parameters			End Parameters		
				Temperature °C	Enthalpy kJ/kg	Dryness	Temperature °C	Enthalpy kJ/kg	Dryness
1	10	200	300	275	1209	−0.15	320	2782	1.04
2	10	300	300	275	1209	−0.15	320	2782	1.04
3	15	300	500	315	1423	−0.19	355	2733	1.12
4	15	400	500	315	1423	−0.19	355	2733	1.12
5	20	400	800	345	1607	−0.49	375	2602	1.35
6	20	500	800	345	1607	−0.49	375	2602	1.35
7	25	400	1000	360	1698		450	2950	
8	25	500	1000	360	1698		450	2950	

In every operation, the system pressure and mass flux were adjusted to the set value by using the bypass valve and the back pressure valve. After the water filled the experimental system, the heat flux was adjusted by using a silicon controlled voltage regulator. When the system pressure, mass flux, and heat flux were fixed, the experiment began. The inlet temperature was increased by increasing the electric power of the test section. Once the outlet temperature reached the experimental requirements or heat transfer deterioration occurred, the experiment was stopped.

2.2. Data Processing

NIST REFPROP is adopted to acquire the corresponding thermal physical parameters, such as enthalpy, and specific heat, by the experimental data.

Due to the high temperature of the test section, the heat dissipation cannot be neglected. Considering that the effective heat will be converted to water enthalpy when the heat transfer is stable, the power efficiency can be calculated by the increase in water enthalpy.

The electric efficiency is calculated by the ratio of the increase in enthalpy to electric power:

$$\eta = \frac{\Delta H}{Q_{\mathrm{E}}} \tag{1}$$

The increase in enthalpy and the electric power can be obtained as follows,

$$\Delta H = H_{\mathrm{out}} - H_{\mathrm{in}} = GA(h_{\mathrm{out}} - h_{\mathrm{in}}) \tag{2}$$

$$Q_{\mathrm{E}} = EI \tag{3}$$

The inner wall heat flux is displayed as follows,

$$q_i = \frac{Q_{\mathrm{E}}\eta}{\pi d_i L} \tag{4}$$

No matter what the enthalpy is, the temperature is fixed in the liquid–gas phase. The electric efficiency should be calculated with the data of the single-phase flow. Many pre-experiments were conducted under different pressures and temperatures. The results show that the electric efficiency varies from 0.85 to 0.95. Higher temperature corresponds to a lower efficiency, and lower temperature corresponds to a higher efficiency. In the current work, the electric efficiency is set to 0.9.

The heat transfer coefficient is defined as

$$\overline{h} = \frac{q}{\overline{t_{iw}} - t_b} \tag{5}$$

where t_{b} is the temperature corresponding to bulk enthalpy. The bulk enthalpy is calculated by

$$H_b = \frac{\iint_S \rho v h ds}{\iint_S 1 ds} \tag{6}$$

where $\overline{t_{\mathrm{iw}}}$ is the average inner wall temperature of a cross-section, it can be obtained by the average temperature of the outer wall. The calculation method refers to the work of Wang [14]. Due to the non-uniform outer wall temperature distribution on the rifled tube, the average of the outer wall temperature is usually used to describe the cross-section outer wall temperature. In addition, the use of average temperature can also reduce the influence of measurement error.

$$\overline{t_{iw}} = \overline{t_{ow}} - \frac{q d_{\mathrm{i}}}{2\lambda_{\mathrm{w}}}\left(\frac{1}{2} - \frac{d_{\mathrm{i}}^2}{d_{\mathrm{o}}^2 - d_{\mathrm{i}}^2}\ln\frac{d_{\mathrm{o}}}{d_{\mathrm{i}}}\right) \tag{7}$$

The dryness is the mass fraction of steam state water in the liquid–gas water and is calculated by

$$x = \frac{H_{\mathrm{b}} - H_{\mathrm{sl}}}{H_{\mathrm{sv}} - H_{\mathrm{sl}}} \times 100\% \tag{8}$$

The average relative error of fitted correlation is calculated as follows

$$error = \frac{Nu_{\mathrm{cal}}}{Nu_{\mathrm{exp}}} - 1 \tag{9}$$

$$error_{\mathrm{average}} = \sum_{i=1}^{n} \frac{error_i}{n} \times 100\% \tag{10}$$

2.3. Uncertainties Analysis

The uncertainties of measurement in the experiment are listed in Table 3. The uncertainty of pressure is decided by the precision of the pressure transmitter (0.25%) and data acquisition board (0.02%). The uncertainty of temperature is determined by the precision of thermocouples and the data acquisition board, the maximum error of thermocouples is 0.5%. The uncertainty of mass flux is mainly induced by the mass flowmeter (0.2%). The uncertainty of inner wall heat flux is estimated by input power and heat dissipation, the precisions of the current transformer and voltage transformer are both 0.5%, and the heat dissipation is considered as 10%.

Table 3. Uncertainties of parameters.

Parameter	Standard Uncertainty
Fluid temperature	0.3 °C
Inner wall temperature	0.4 °C
Pressure	0.006 MPa
Mass flux	6.2 kg/(m^2·s)
Inner wall heat flux	21.2 kW/m^2

3. Results and Discussion

3.1. The Heat Transfer Characteristics of Water in the Smooth Tube

3.1.1. The Heat Transfer Characteristics at Subcritical Pressure

The heat transfer characteristics of water in the smooth tube at subcritical pressure are shown in Figure 6. The effect degree of heat flux on wall temperature varies with the pressure and mass flux, yet the trends are the same. When the pressure and mass flux are fixed, the critical dryness for the heat transfer deterioration will decrease with the increase in heat flux. Meanwhile, the peak temperature rises. It can be seen in Figure 6 that HTD occurs in advance as the heat flux increases. The reason for this phenomenon is that as the heat flux increases, more heat is released from the wall. The wall cannot be cooled effectively by the bulk fluid, which results in an advance in HTD and an increase in the temperature peak. In addition, the critical dryness is advanced as the system pressure increases. The critical dryness at 10 MPa are larger than 0.5, and the HTD types are dryout (DO). DO is an HTD type that happens in the high-dryness region. DO occurs when there is only a few liquid water near the inner wall and they cannot effectively absorb the heat from the wall. On the contrary, the critical dryness at 15 MPa are smaller than 0.5, and the HTD types are deviation nuclear boiling (DNB). DNB is another HTD type that occurs in the low dryness region when the bubble cannot escape from the wall effectively. This phenomenon occurs because the density gap between the vapor phase and the liquid phase decreases with the increase in the pressure. With the decrease in the density gap, it is more difficult for the bubble to escape from the wall, which leads to the advance in HTD. Under these operating conditions, wall temperatures stay stable during the nucleate boiling process until the occurrence of HTD.

Figure 7 shows the heat transfer coefficient (HTC) distributions of the smooth tube at the subcritical pressure. HTC increases as the bulk enthalpy increases and reaches the peak during the nucleate boiling process. This phenomenon indicates that the nucleate boiling has a strong heat transfer ability. It can be seen that HTC increases with the increase in heat flux until HTD occurs. In addition, HTD occurs in advance as heat flux increases, which results in the decrease in HTC. The increase in heat flux not only enhances the ability of nucleate boiling but also changes the critical dryness for HTD.

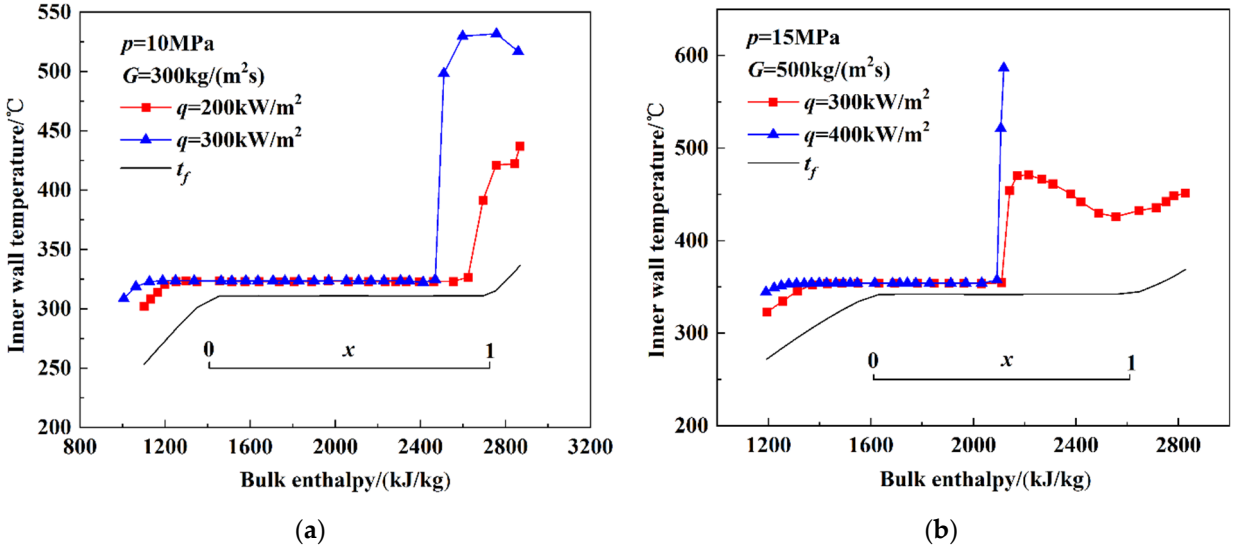

(**a**) (**b**)

Figure 6. Inner wall temperature distributions of the smooth tube at subcritical pressure ((**a**) 10 MPa, (**b**) 15 MPa).

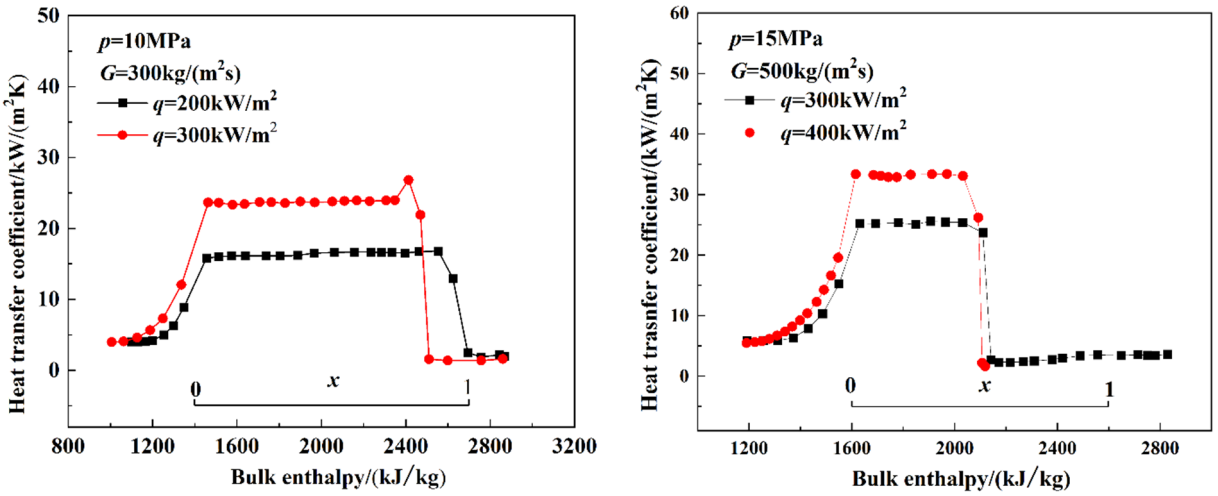

(**a**) (**b**)

Figure 7. Heat transfer coefficient distributions of the smooth tube at subcritical pressure ((**a**) 10 MPa, (**b**) 15 MPa).

3.1.2. The Heat Transfer Characteristics at Near-Critical Pressure

The inner wall temperature distributions at near-critical pressure are displayed in Figure 8. HTD occurs at both 400 and 500 kW/m^2 heat flux, with the critical dryness values of 0.39 and 0.25, respectively. Therefore, the HTD types both belong to DNB. The maximum increases in the wall temperature after HTD occur are 6 °C and 36 °C, respectively, which means that the inner wall temperature increases and the HTD occurs easily with the increase in heat flux. In addition, it can also be seen that the wall temperature drops after HTD occurs, which indicates heat transfer recovery.

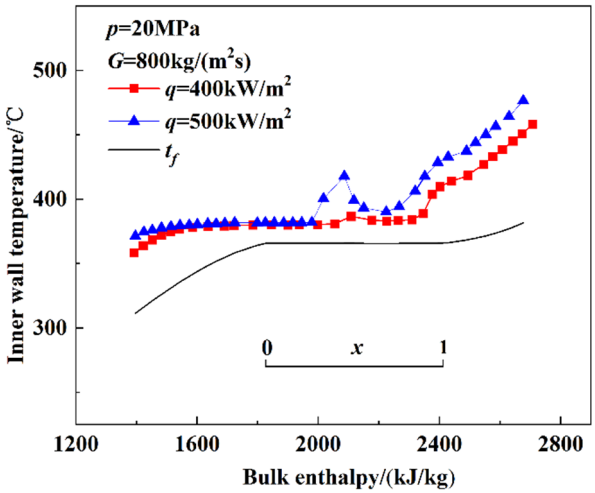

Figure 8. Inner wall temperature distributions of the smooth tube at near-critical pressure.

Figure 9 shows the HTC distributions of water in the smooth tube at near-critical pressure. The influence of heat flux is small in the low and high bulk enthalpy regions, whereas the HTCs for the different heat fluxes are similar. Only in the liquid–gas phase region does the difference caused by heat flux appear. HTC remains stable during the nucleate boiling process at near-critical pressure, which is the same as the HTC at subcritical pressure. Meanwhile, HTD occurs more easily at higher heat flux. Unlike the subcritical pressure, the HTC will gradually improve after HTD occurs, which may result from the high velocity of water that enhances the convective flow and improves the heat transfer performance.

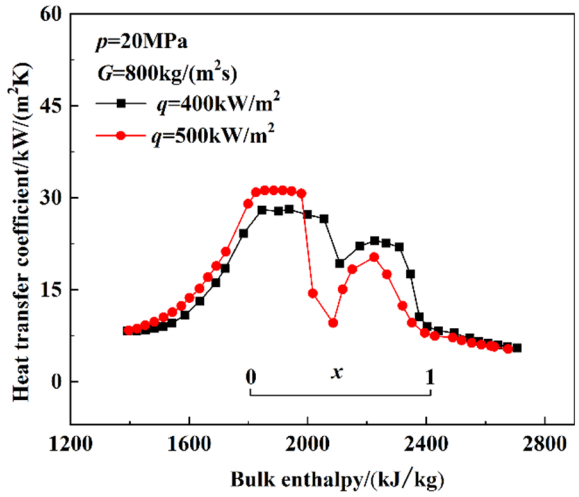

Figure 9. Heat transfer coefficient distributions of the smooth tube at near-critical pressure.

3.1.3. The Heat Transfer Characteristics at Supercritical Pressure

Figure 10 shows the inner wall temperature distributions at supercritical pressure. Unlike the subcritical pressure and near-critical pressure, the inner wall temperature increases with the increase in bulk enthalpy. This phenomenon results from the supercritical water characteristics that supercritical water has no obvious boundary between vapor phase and liquid phase. Instead of a liquid–gas boundary, there is an enthalpy region where the thermophysical properties vary dramatically. The distributions of thermophysical properties at 27 MPa are shown in Figure 11, they are obtained by software NIST REFPROP. Due to the high specific heat in the pseudo-critical region, the wall temperature increases slowly, and it means enhancement of heat transfer (HTE). Heat flux and mass flux will affect the variation degrees of thermophysical properties and then result in different heat transfer performances. HTD will occur when q/G is big, and HTE will occur when q/G is small.

HTD mainly results from the dramatic variation of specific heat, density, viscosity, etc. When HTD occurs, the bulk temperature is smaller than the pseudo-critical temperature, and the inner wall temperature is bigger than it. In addition, the curve of temperature in the high enthalpy region is steeper than in low enthalpy region, which indicates that the heat transfer characteristics in the low enthalpy region are better.

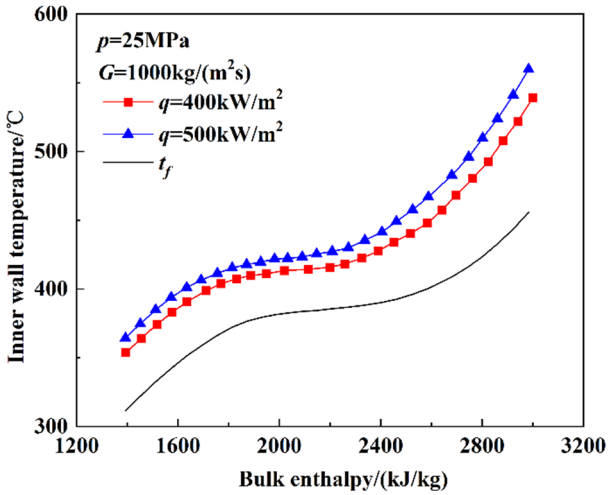

Figure 10. Inner wall temperature distributions of the smooth tube at supercritical pressure.

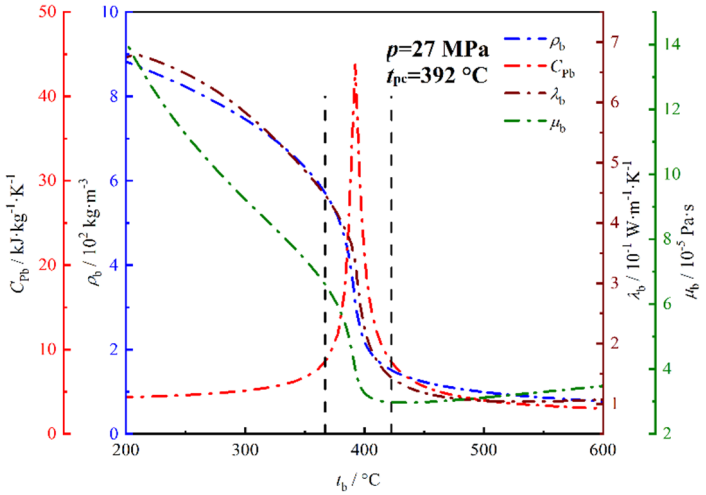

Figure 11. Thermophysical properties of supercritical water at 27 MPa.

By comparing the inner wall temperature at different heat fluxes, it can be seen that the inner wall temperature increases with the increase of heat flux. Moreover, the increase in temperature in the low enthalpy region is smaller than that in the high enthalpy region, which reveals that the effect of heat flux in the high enthalpy region is bigger than that in the low enthalpy region. Therefore, reducing the heat flux is an effective method to improve the heat transfer performance and reduce the wall temperature.

Figure 12 displays the HTC distributions at the supercritical pressure. When the mass flux and pressure are fixed, heat flux has little effect on the HTC in low enthalpy region, and the HTC is mainly affected by mass flux. As the increase in bulk enthalpy, the influence of heat flux on HTC gradually appears. In addition, it can also be seen that the heat transfer performance under 400 kW/m^2 is better than 500 kW/m^2. The difference in inner wall temperature distribution is also the phenomenon of the heat transfer characteristics of supercritical water. The peak of HTC is located near the pseudo-critical enthalpy; besides, there is no dramatic temperature rise. Therefore, the convective heat transfer presents HTE phenomenon. As mentioned above, the HTC decreases more sharply in the high enthalpy

region than in the low enthalpy region; the heat transfer characteristics of pseudo liquid are better than pseudo gas.

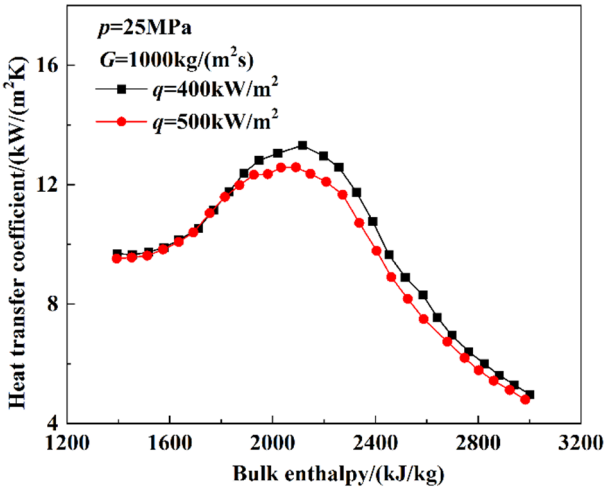

Figure 12. Heat transfer coefficients of the smooth tube at supercritical pressure.

3.2. The Heat Transfer Characteristics of Water in the Rifled Tube

3.2.1. The Heat Transfer Characteristics at Subcritical Pressure

Inner wall temperature distributions of the rifled tube at subcritical pressure are shown in Figure 13. As same as the smooth tube, the influence of heat flux on the heat transfer characteristics in the rifled tube displays different degrees under different operating parameters, such as pressure and mass flux, yet the tendency is similar. The critical dryness decreases as heat flux increases; therefore, heat transfer performance can be improved by reducing heat flux. Different from the smooth tube, the critical dryness for the rifled tube are bigger than 0.7, HTD both belong to DO type. Moreover, the critical dryness is delayed by using the rifled tube. This phenomenon is induced by the following reasons that have been analyzed in our previous work [15]. First, the centrifugal force produced by the internal thread throws the cold fluid onto the inner wall, which enhances the cooling effect of water. Second, the internal thread reduces the boundary layer thickness and makes the boundary layer separated, which makes the fluid mix uniformly. Finally, the existence of an internal thread increases the contact area between water and the inner wall. Therefore, the use of the rifled tube can effectively enhance the heat transfer characteristics between water and wall, then delays and prevents HTD.

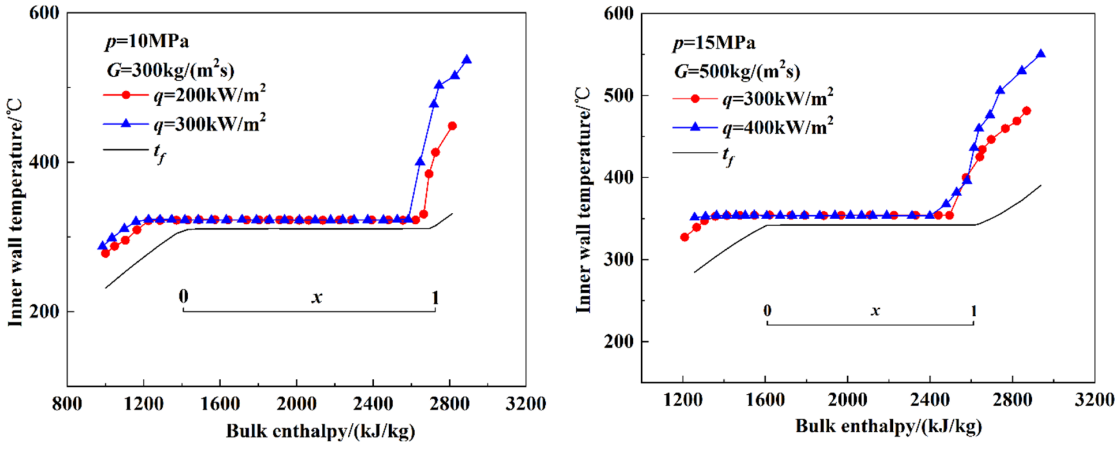

Figure 13. Inner wall temperature distributions of the rifled tube at subcritical pressure ((**a**) 10 MPa, (**b**) 15 MPa).

The HTC distributions of the rifled tube at subcritical pressure are displayed in Figure 14. Similar to the smooth tube, the influence of heat flux on the HTC in the low enthalpy region is small. The HTC increases gradually and finally reaches a maximum as the enthalpy increases. It is found that the peak value of HTC increases with the heat flux. However, the critical dryness increases and HTD occurs in advance.

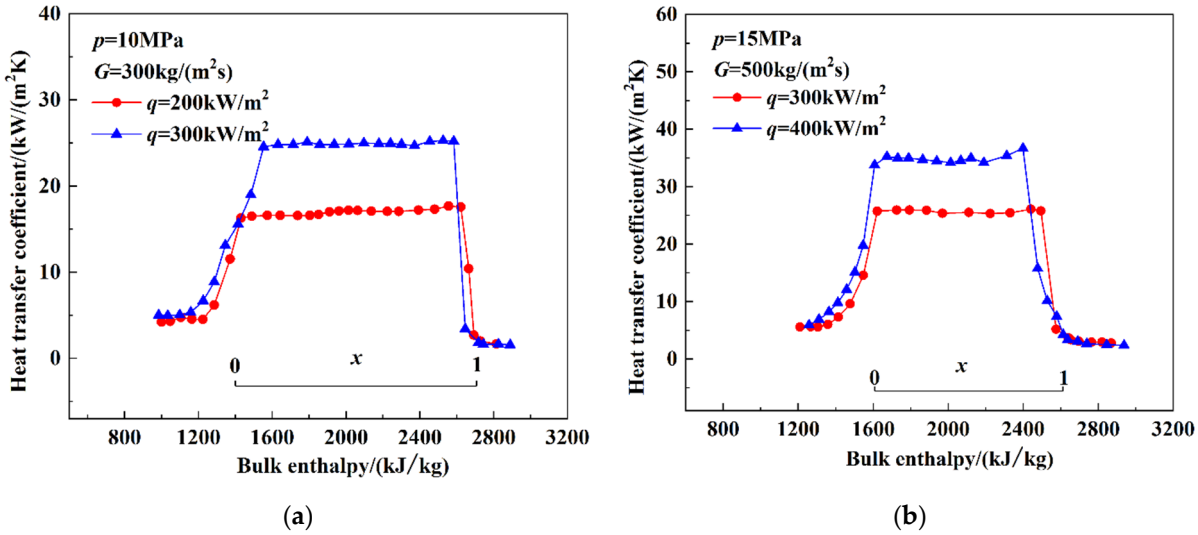

(**a**) (**b**)

Figure 14. Heat transfer coefficient distributions of the rifled tube at subcritical pressure ((**a**) 10 MPa, (**b**) 15 MPa).

3.2.2. The Heat Transfer Characteristics at Near-Critical Pressure

Figure 15 displays the inner wall temperature distributions of the rifled tube at near-critical pressure. Different from the smooth tube, the inner wall temperature of the rifled tube does not display the DNB characteristics as the smooth tube. The critical dryness for HTD are both larger than 0.7, so the DNB types belong to DO. This phenomenon is mentioned above. In addition, the wall temperature increases as the heat flux increases when HTD occurs.

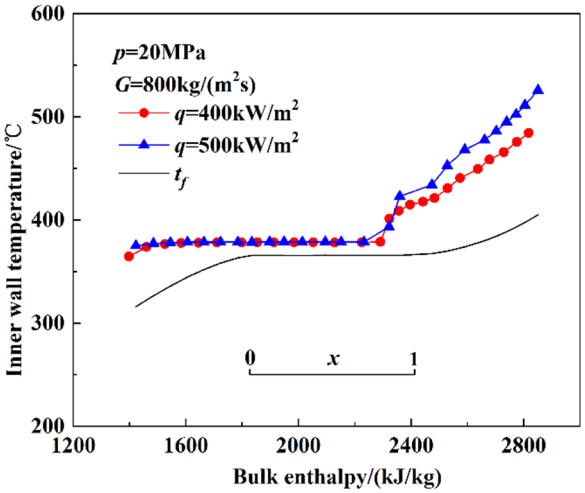

Figure 15. Inner wall temperature distributions of the rifled tube at near-critical pressure.

The HTC distributions of water in the rifled tube at near-critical pressure are shown in Figure 16. The influence of heat flux is mainly reflected in liquid–gas boiling region, where the HTC increases with the increase in heat flux. The HTC distributions of water in the smooth tube and rifled tube in the low- and high-enthalpy regions are similar.

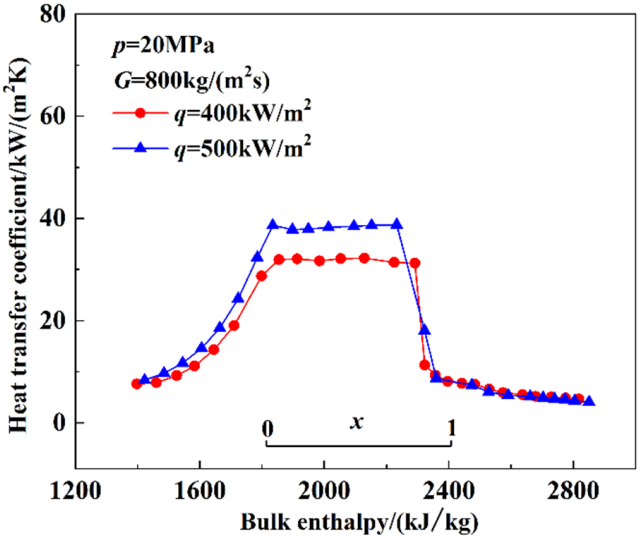

Figure 16. Heat transfer coefficient distributions of the rifled tube at near-critical pressure.

3.2.3. The Heat Transfer Characteristics at Supercritical Pressure

As shown in Figure 17, the tendencies of the inner wall temperature for the rifled tube are the same as that for the smooth tube. The inner wall temperature increases with the heat flux. The increasing degree in the low-enthalpy region is small, yet it is big in high enthalpy region.

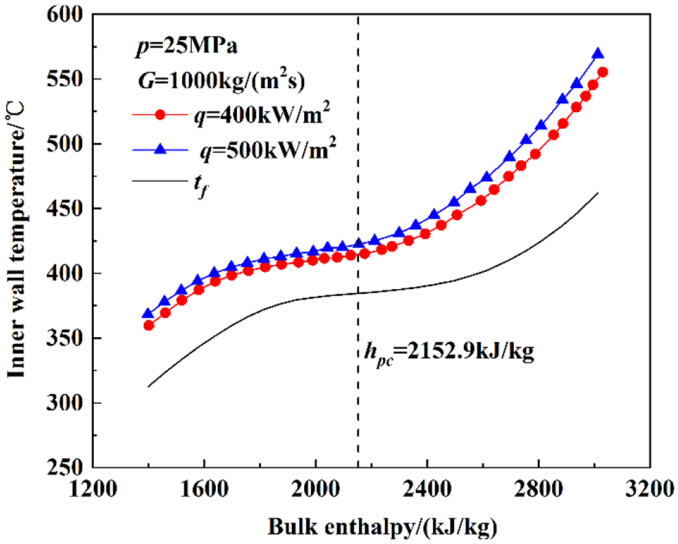

Figure 17. Inner wall temperature distributions of the rifled tube at supercritical pressure.

The HTC distributions of the rifled tube show different characteristics from the smooth tube, which is displayed in Figure 18. On one hand, the influence of the heat flux for the rifled tube is mainly reflected in the low enthalpy region, yet for the smooth tube it is mainly reflected in the pseudo-critical region and the high enthalpy region. On the other hand, the HTCs for the rifled tube are both larger than the smooth tube in all enthalpy regions. This phenomenon mainly results from the enhanced heat transfer performance produced by the internal thread.

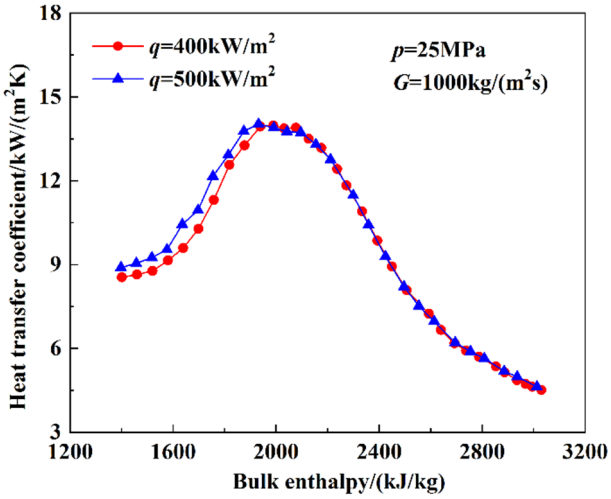

Figure 18. Heat transfer coefficient distributions of the rifled tube at a supercritical pressure.

3.3. Heat Transfer Correlations

3.3.1. Heat Transfer Correlations at Subcritical Pressure

The heat transfer performance has obvious differences in both the single-phase region and the two-phase region. The two-phase region can be divided into the normal heat-transfer region and the DO region; the flow pattern in the normal heat transfer region is annular flow, and the flow pattern in the DO region is sprat flow. Therefore, the fitting of the two-phase heat transfer correlation should be performed separately. Finally, the data are handled respectively in the single-phase region, the two-phase normal heat transfer region, and the DO region. The heat transfer correlations are listed as follows.

The Dittus–Boelter correlation is adopted for the heat transfer coefficient calculation of single-phase water [16]. The heat transfer coefficient for the smooth tube and rifled tube can both be fitted with the experimental data according to the D–B correlation.

$$Nu = 0.023 Re^{0.8} Pr^{0.4} \tag{11}$$

The heat transfer correlations of single-phase water are listed as follows:

$$\text{Smooth tube}: \ Nu = 0.12157 Re^{0.65081} Pr^{0.85075} \tag{12}$$

$$\text{Rifled tube}: \ Nu = 2.6657 Re^{0.42278} Pr^{3.46485} \tag{13}$$

The average relative error of the smooth tube is 9.5%, and that of the rifled tube is 7.8%. The correlations can be used at subcritical pressure, 300–500 kg/(m^2·s) mass flux, and 200–400 kW/m^2 heat flux. Under these operating conditions, the *Re* of the smooth tube varies from 40,000 to 130,000, the *Re* of the rifled tube varies from 40,000 to 130,000, and *Pr* varies from 0.82 to 1.16. Figure 19 shows the comparisons between fitted correlation and experimental data.

A well known two-phase forced convective heat transfer correlation with X_{tt} proposed by Lockhart with Martinelli is used to fit the correlations of the liquid–gas phase normal heat transfer [17].

$$\frac{h_{tp}}{h_l} = f\left(\frac{1}{X_{tt}}\right) \tag{14}$$

When the flow belongs to turbulent flow, X_{tt} can be defined by

$$X_{tt} = \left(\frac{1-x}{x}\right)^{0.9} \left(\frac{\rho_g}{\rho_l}\right)^{0.5} \left(\frac{\mu_l}{\mu_g}\right)^{0.1} \tag{15}$$

Considering the influence of pressure, mass flux and heat flux, the heat transfer correlation can be fitted by

$$\frac{h_{tp}}{h_l} = a\frac{1}{X_{tt}{}^b}\left(\frac{p}{p_{cr}}\right)^c\left(\frac{G}{G_{max}}\right)^d q^e \tag{16}$$

Finally, the heat transfer correlations of two phases with normal heat transfer are listed as follows:

Smooth tube :

$$\frac{h_{tp}}{h_l} = 0.0074 \cdot \left(\frac{1}{X_{tt}}\right)^{0.00333} \cdot \left(\frac{p}{p_{cr}}\right)^{0.32711} \cdot \left(\frac{G}{G_{max}}\right)^{-1.23559} \cdot q^{0.93435} \tag{17}$$

Refiled tube :

$$\frac{h_{tp}}{h_l} = 0.00219 \cdot \left(\frac{1}{X_{tt}}\right)^{0.00385} \cdot \left(\frac{p}{p_{cr}}\right)^{-2.18713} \cdot \left(\frac{G}{G_{max}}\right)^{-0.32309} \cdot q^{0.91228} \tag{18}$$

The average relative error of the smooth tube is 12.9%, and that of the rifled tube is 14.2%. The correlations can be used at subcritical pressure, 300–500 kg/(m^2·s) mass flux, and 200–400 kW/m^2 heat flux.

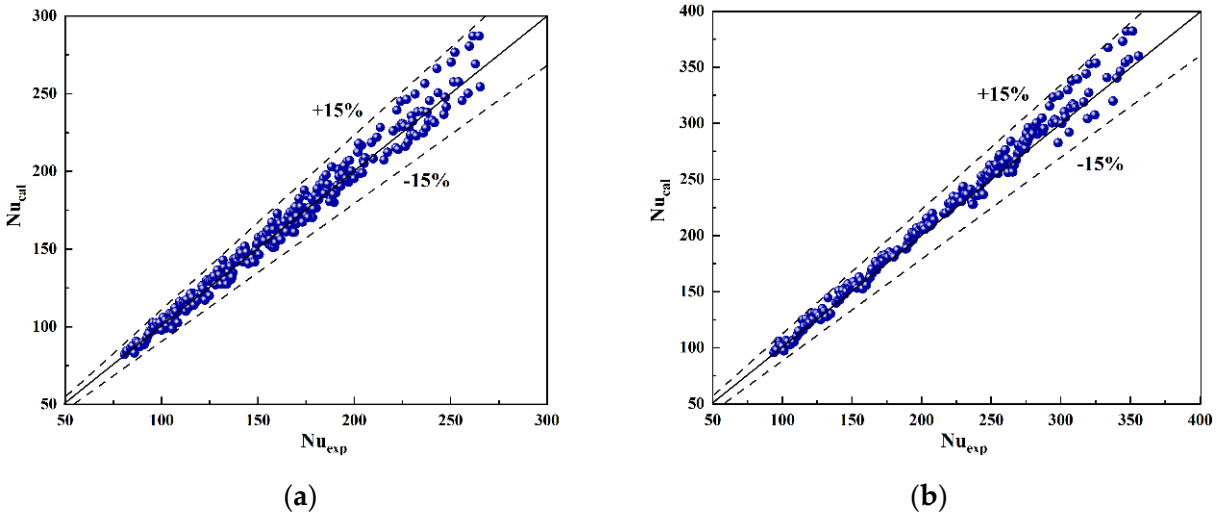

(**a**) (**b**)

Figure 19. Comparisons of *Nu* between experiment data and fitted correlations at subcritical pressure ((**a**) smooth tube, (**b**) rifled tube).

The heat transfer correlations for the DO region are obtained by empirical correlation proposed by Slaughterback [18]. The fitted correlations are listed as follows:

Smooth tube :

$$Nu = 5.61676 \times 10^{-8} \cdot \left(Re_g\left(x + \frac{\rho_g}{\rho_l}(1-x)\right)\right)^{0.88281} Pr_{gw}{}^{3.55268} \cdot q^{1.37097}\left(\frac{\lambda_g}{\lambda_{cr}}\right)^{-1.53717} \tag{19}$$

Refiled tube :

$$Nu = 0.29048 \cdot \left(Re_g\left(x + \frac{\rho_g}{\rho_l}(1-x)\right)\right)^{0.70831} Pr_{gw}{}^{0.13321} \cdot q^{-0.29783} \tag{20}$$

The average relative error of the smooth tube is 15.1%, and that of the rifled tube is 16.8%. The correlations can be used at subcritical pressure, 300–500 kg/(m^2·s) mass flux, and 200–400 kW/m^2 heat flux. Under these operating conditions, the Re_g of smooth tube varies from 275,000 to 395,000, the Re_g of the rifled tube varies from 194,000 to 408,000, the Pr_{gw} of the smooth tube varies from 0.97 to 1.17, and the Pr_{gw} of the rifled tube varies from 0.96 to 1.41.

3.3.2. Heat Transfer Correlations at Near-Critical Pressure

The method for fitting heat transfer correlation of near-critical pressure is the same as the subcritical pressure.

The heat transfer correlations of a single phase are as follows:

$$\text{Smooth tube}: \ Nu = 0.12157 Re^{0.65081} Pr^{0.85075} \tag{21}$$

$$\text{Rifled tube}: \ Nu = 2.6657 Re^{0.42278} Pr^{3.46485} \tag{22}$$

The average relative error of the smooth tube is 7.1%, and that of the rifled tube is 8.5%. The correlations can be used at near-critical pressure, 800 kg/(m^2·s) mass flux, and 400–500 kW/m^2 heat flux. Under these operating conditions, the *Re* of smooth tube varies from 190,000 to 270,000, that of the *Re* of rifled tube varies from 190,000 to 260,000, and that of *Pr* varies from 0.87 to 1.72. Figure 20 shows the comparisons between experimental data and the fitted correlations.

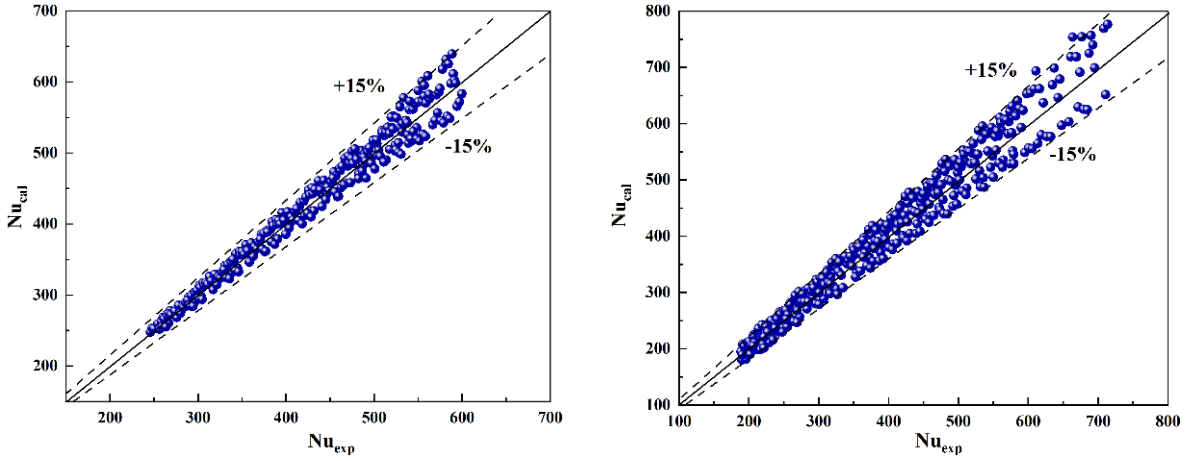

(**a**) (**b**)

Figure 20. Comparisons of *Nu* between experimental data and fitted correlations at near-critical pressure ((**a**) smooth tube, (**b**) rifled tube).

The heat transfer correlations of two phases with normal heat transfer are as follows:

$$\text{Smooth tube}: \ \frac{h_{tp}}{h_l} = 0.01126 \cdot \left(\frac{1}{X_{tt}}\right)^{-0.01253} \cdot \left(\frac{p}{p_{cr}}\right)^{0.44886} \cdot \left(\frac{G}{G_{max}}\right)^{-0.82915} \cdot q^{0.5421} \tag{23}$$

$$\text{Rifled tube}: \ \frac{h_{tp}}{h_l} = 5.37542 \cdot \left(\frac{1}{X_{tt}}\right)^{-0.00988} \cdot \left(\frac{p}{p_{cr}}\right)^{1.36723} \cdot \left(\frac{G}{G_{max}}\right)^{10.20153} \tag{24}$$

The average relative error of the smooth tube is 14.8%, and that of the rifled tube is 13.4%. The correlations can be used at near-critical pressure, 800 kg/(m^2·s) mass flux, and 400–500 kW/m^2 heat flux.

The heat transfer correlations of the DO region are as follows:

Smooth tube :

$$Nu = 3.58542 \times 10^{-4} \cdot \left(Re_g\left(x + \tfrac{\rho_g}{\rho_l}(1-x)\right)\right)^{1.12155} {Pr_{gw}}^{0.76758} \cdot q^{-0.1074} \tag{25}$$

Rifled tube :

$$Nu = 0.000122923 \cdot \left(Re_g\left(x + \tfrac{\rho_g}{\rho_l}(1-x)\right)\right)^{0.59747} {Pr_{gw}}^{4.97401} \cdot q^{0.72153} \left(\tfrac{\lambda_g}{\lambda_{cr}}\right)^{-1.51281} \tag{26}$$

The average relative error of the smooth tube is 17.9%, and that of the rifled tube is 17.3%. The correlations can be used at near-critical pressure, 800 kg/(m^2·s) mass flux, and 400–500 kW/m^2 heat flux. Under these operating conditions, the Re_g of the smooth tube is 607,000, that of the Re_g of the rifled tube is 577,000, the Pr_{gw} of the smooth tube varies from 1.15 to 1.56, and that of the Pr_{gw} of the rifled tube varies from 1.05 to 1.56.

3.3.3. Heat Transfer Correlations at Supercritical Pressure

The heat transfer characteristics at supercritical pressure display a different trend near the pseudo critical temperature. It can be seen from the experimental results that the HTC before the pseudo-critical temperature is bigger than that after the pseudo-critical temperature. Therefore, the heat transfer correlations are divided into high enthalpy and low enthalpy regions. Meanwhile, the specific volume ratio and average specific heat are used to modify the correlations. The fitted correlations are listed as follows:

Smooth tube:

$$Nu = 0.00787 Re_f^{0.86279} \cdot \left(\frac{h_w - h_f}{t_w - t_f} \cdot \frac{\mu_f}{k_f}\right)^{0.31476} \cdot \left(\frac{v_f}{v_w}\right)^{0.14877} \text{(before pseudo} - \text{critical temperature)} \quad (27)$$

$$Nu = 0.00021831 Re_f^{1.14444} \cdot \left(\frac{h_w - h_f}{t_w - t_f} \cdot \frac{\mu_f}{k_f}\right)^{0.44217} \cdot \left(\frac{v_f}{v_w}\right)^{0.38013} \text{(after pseudo} - \text{critical temperature)} \quad (28)$$

Rifled tube:

$$Nu = 0.00021831759412 Re_f^{1.03882} \cdot \left(\frac{h_w - h_f}{t_w - t_f} \cdot \frac{\mu_f}{k_f}\right)^{0.41854} \cdot \left(\frac{v_f}{v_w}\right)^{0.12671} \text{(before pseudo} - \text{critical temperature)} \quad (29)$$

$$Nu = 0.02824 Re_f^{0.76941} \cdot \left(\frac{h_w - h_f}{t_w - t_f} \cdot \frac{\mu_f}{k_f}\right)^{0.00209} \cdot \left(\frac{v_f}{v_w}\right)^{-0.02634} \text{(after pseudo} - \text{critical temperature)} \quad (30)$$

The average relative errors of the smooth tube are 9.5% and 10.7% and that of the rifled tube is 8.4% and 7.9%. The correlations can be used in supercritical pressure, 1000 kg/(m^2·s) mass flux, and 400–500 kW/m^2 heat flux. When bulk fluid is below the pseudo-critical temperature, Re_f of the smooth tube varies from 283,000 to 450,000, and Re_f of the rifled tube varies from 226,000 to 389,000. When the bulk fluid is above the pseudo-critical temperature, the Re_f of the smooth tube varies from 483,000 to 727,000, the Re_f of rifled tube varies from 405,000 to 691,000. Figure 21 shows comparisons of Nu between fitted correlation and experiments.

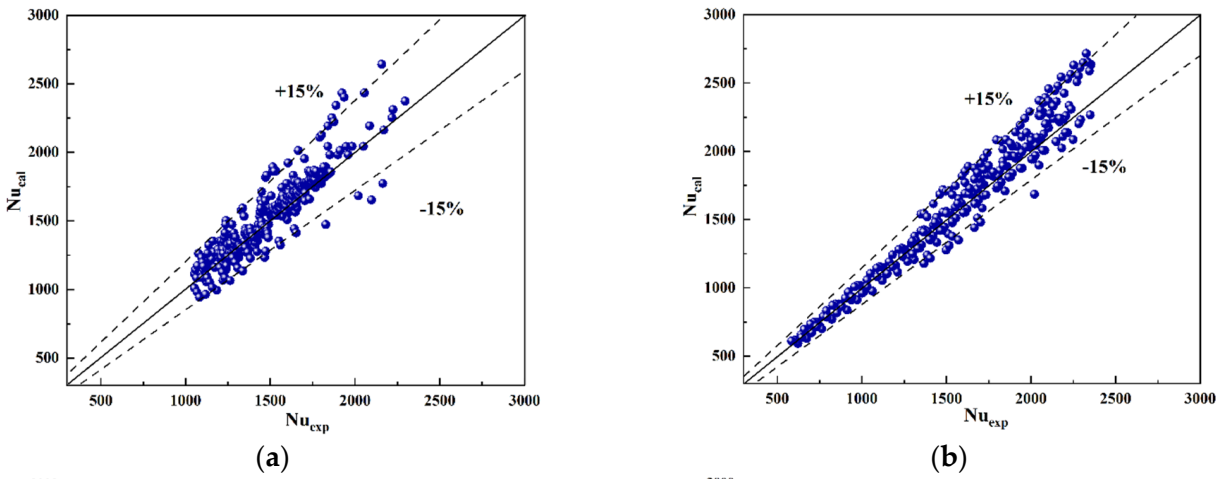

Figure 21. *Cont.*

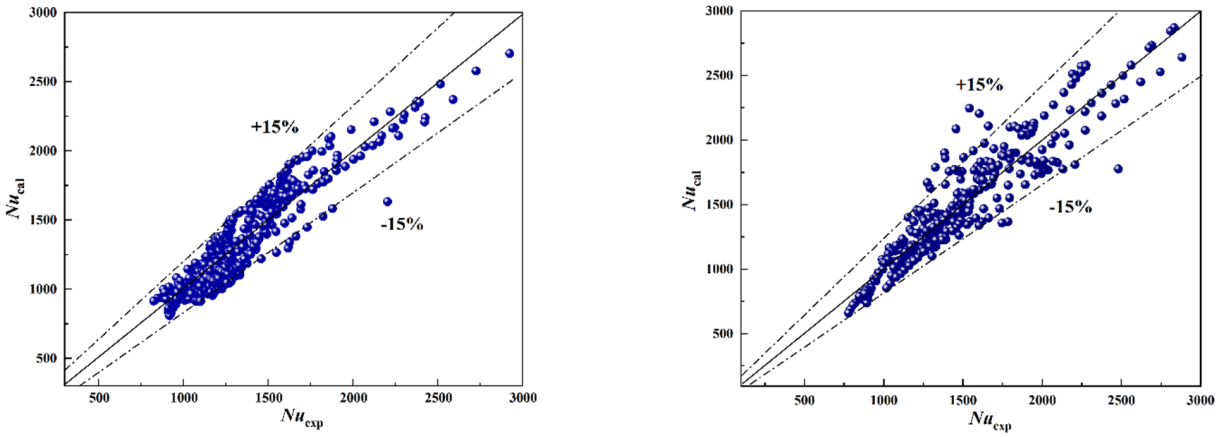

Figure 21. Comparisons of *Nu* between experimental data and fitted correlations at supercritical pressure ((**a**) smooth tube before pseudo-critical region, (**b**) smooth tube after pseudo-critical region, (**c**) rifled tube before pseudo-critical region, (**d**) rifled tube after pseudo-critical region).

3.4. The Resistance Characteristics

3.4.1. The Resistance Characteristics at Subcritical/Near-Critical Pressure

The friction resistance coefficients are calculated by a single phase (single-phase water and single-phase steam) and by two phases. The friction resistance coefficient correlations of single-phase water and single-phase steam are fitted by the correlation proposed by Blasius.

$$f = \mathrm{A}Re^{\mathrm{B}}\left(\frac{G}{500}\right)^{\mathrm{C}} \tag{31}$$

The friction resistance coefficient correlations fitted by the experimental data are listed as follows:

$$\text{Smooth tube}: \ f = 0.00040028Re^{0.32928}\left(\frac{G}{500}\right)^{-0.91558} \tag{32}$$

$$\text{Rifled tube}: \ f = 0.03602Re^{-0.06068}\left(\frac{G}{500}\right)^{-1.45922} \tag{33}$$

The average relative error of the smooth tube is 13.7%, and that of the rifled tube is 19.5%. The correlations can be used at subcritical/near-critical pressure, 300–800 kg/(m^2·s), and 200–500 kW/m^2 heat flux. Under these operating conditions, the *Re* of smooth tube varies from 40,000 to 260,000, and the *Re* of rifled tube varies from 40,000 to 250,000.

Usually, the friction resistance coefficients of two phases are calculated through the two-phase friction ratio with the single-phase friction resistance coefficient.

$$\Delta P_{\mathrm{TP}} = \phi_{\mathrm{LO}}^2 \cdot \Delta P_{\mathrm{LO}} \tag{34}$$

$$\phi_{\mathrm{LO}}{}^2 = 1 + f(x, P, G, \ldots) \cdot \left(\frac{\rho_{\mathrm{l}}}{\rho_{\mathrm{g}}} - 1\right) \tag{35}$$

$$f(x, P) = \frac{\phi_{\mathrm{LO}}{}^2 - 1}{\frac{\rho_{\mathrm{l}}}{\rho_{\mathrm{g}}} - 1} \tag{36}$$

The $f(x,P)$ is fitted according to $C = C_0x^{\mathrm{n}}(1-x)^{\mathrm{m}}$, and the fitted correlations are listed as follows:

$$\text{Smooth tube}: \ C(x) = 15.40898 \cdot x^{2.81962} \cdot (1-x)^{5.20519} \tag{37}$$

$$\text{Rifled tube}: \ C(x) = 7.66784 \cdot x^{2.32437} \cdot (1-x)^{2.32437} \tag{38}$$

The average relative error of the smooth tube is 8.1%, and that of the rifled tube is 8.8%. The correlations can be used at subcritical/near-critical pressure, 300–800 kg/(m^2·s),

and 200–500 kW/m^2 heat flux. Figure 22 shows the comparisons of the two-phase friction resistance coefficient between the fitted correlations and experimental data.

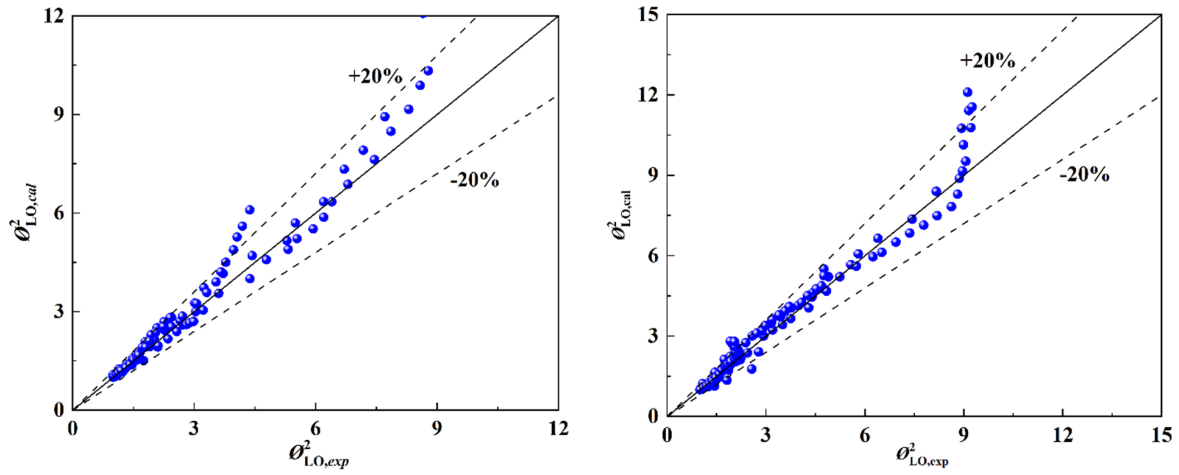

Figure 22. Comparisons of two-phase friction resistance coefficient between experimental data and fitted correlations at the subcritical/near-critical pressure ((**a**) smooth tube, (**b**) rifled tube).

3.4.2. The Resistance Characteristics at Supercritical Pressure

The friction resistance coefficient distributions at supercritical pressure are shown in Figure 23. The friction resistance coefficient has an obvious increase near the pseudo-critical temperature. Therefore, the distribution of friction resistance coefficient is induced by the thermophysical variation.

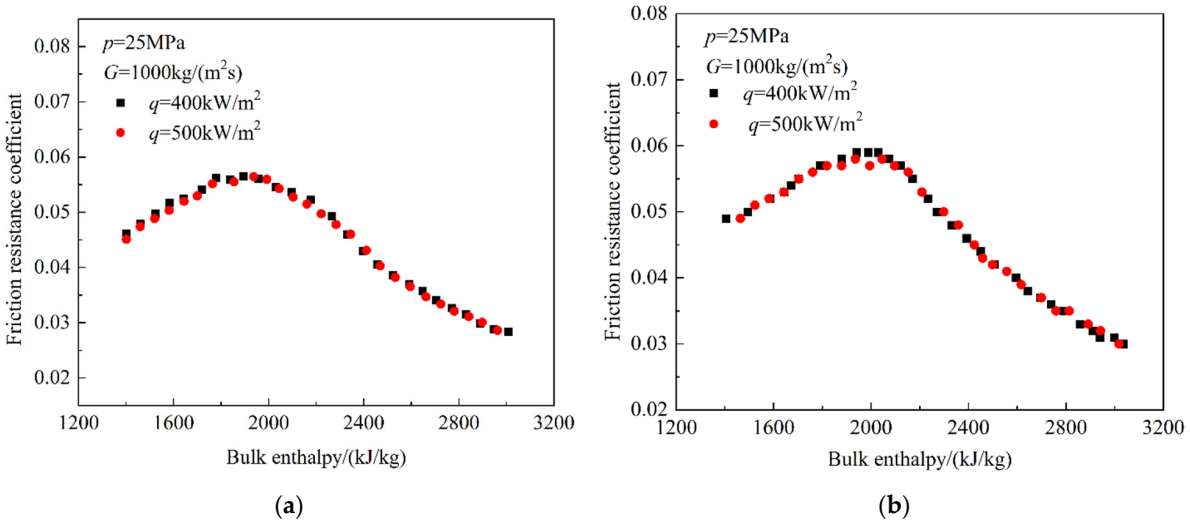

Figure 23. The friction resistance coefficient distributions at supercritical pressure ((**a**) smooth tube; (**b**) rifled tube).

Considering the different trends before and after pseudo-critical temperature, the correlations of friction resistance coefficient can be divided into the low-enthalpy region and the high-enthalpy region. Meanwhile, the influences of mass flux and *Re* should be considered. Finally, the fitted correlations are listed as follows:

Smooth tube:

$$f = 0.00861Re^{0.14383}\left(\frac{G}{1000}\right)^{-1.2493} \quad \text{(before pseudo} - \text{critical temperature)} \tag{39}$$

$$f = 1.613084 \times 10^5 Re^{-1.14237} \left(\frac{G}{1000}\right)^{-4.69174} \quad (\text{after pseudo} - \text{critical temperature}) \quad (40)$$

Rifled tube:

$$f = 0.00611 Re^{0.17381} \left(\frac{G}{1000}\right)^{-4.06717} \quad (\text{before pseudo} - \text{critical temperature}) \quad (41)$$

$$f = 2.86103 \times 10^8 Re^{-1.70078} \left(\frac{G}{1000}\right)^{-1.01076} \quad (\text{after pseudo} - \text{critical temperature}) \quad (42)$$

The average relative errors of the smooth tube are 11.7% and 8.8%, and those of the rifled tube are 8.5% and 12.9%. The correlations can be used at supercritical pressure, 1000 kg/(m^2·s), and 400–500 kW/m^2 heat flux. When bulk fluid is below the pseudo-critical temperature, the *Re* of smooth tube varies from 280,000 to 450,000, and the *Re* of the rifled tube varies from 230,000 to 389,000. When bulk fluid is above the pseudo-critical temperature, the *Re* of the smooth tube varies from 480,000 to 730,000, and the *Re* of the rifled tube varies from 400,000 to 690,000. Figure 24 shows the comparisons between fitted correlations and experimental data.

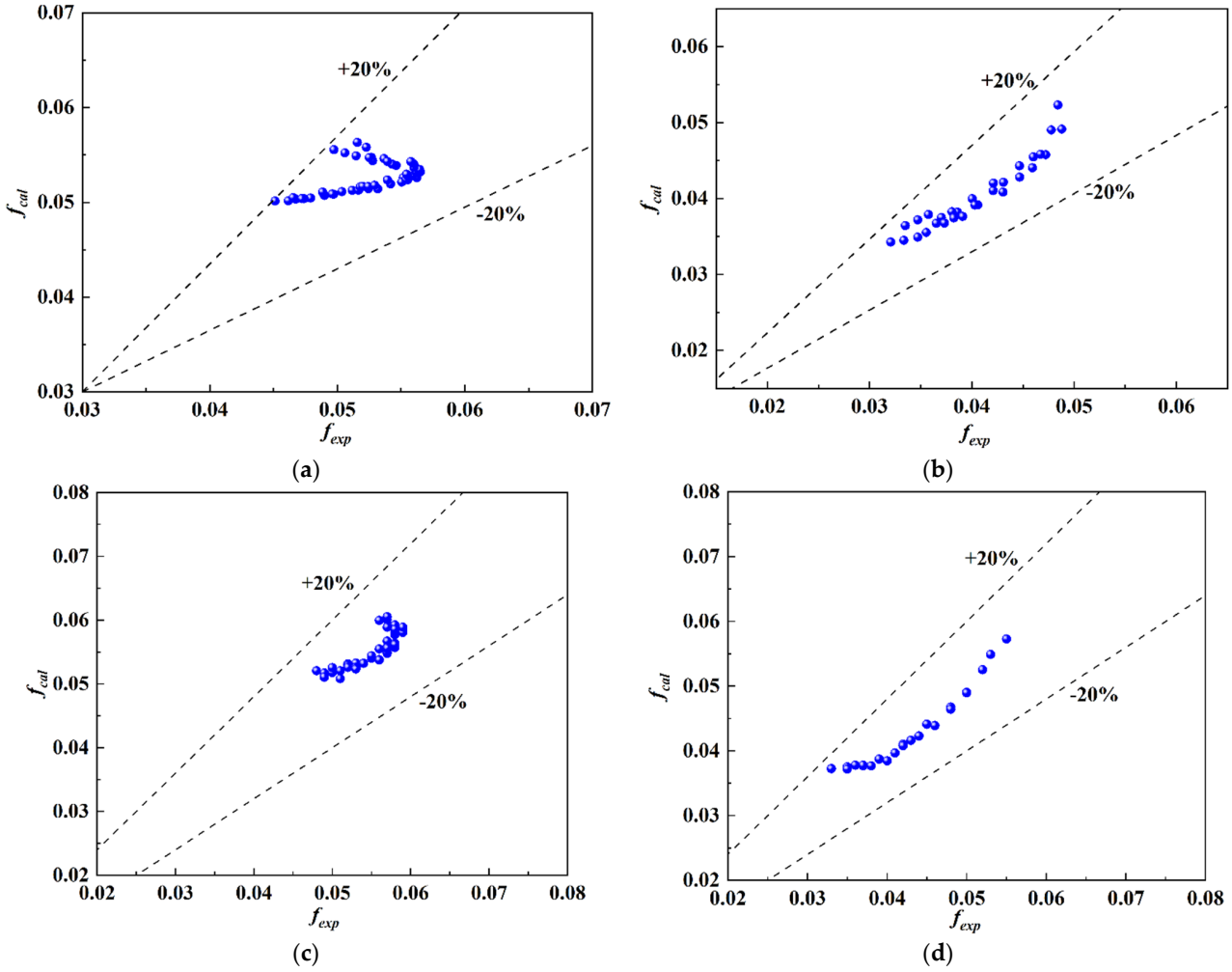

Figure 24. The comparisons of friction resistance coefficient between experimental data and fitted correlations at supercritical pressure ((**a**) smooth tube in the low-enthalpy region; (**b**) smooth tube in the high-enthalpy region; (**c**) rifled tube in the low-enthalpy region; (**d**) rifled tube in the high-enthalpy region).

4. Conclusions

The study of heat transfer and flow-resistance characteristics is the key to a supercritical boiler and has important significance in water wall design and boiler operation. The experiments were conducted in the high-temperature and high-pressure experimental system of Xi'an Jiaotong University. The operating parameter range was such that the pressure range was 10–25 MPa, heat flux was 200–500 kW/m^2, and mass flux was 300–1000 kg/(m^2·s). The main conclusions are summarized as follows:

1. At subcritical pressures, the inner wall temperature increased with enthalpy in the low enthalpy region, the inner wall temperature remained stable in the nucleate boiling region, and the inner wall temperature abruptly increased after HTD occurred. The HTC was improved, and HTD occurred in advance with the increase in heat flux. In addition, the HTC could be improved, and HTD could be delayed by using the rifled tube.
2. At near-critical pressure, the heat transfer characteristics were similar to those at the subcritical pressure. However, DNB was more likely to occur. The peak temperature increased as the heat flux increased. DNB could be avoided, and the HTC could be improved by using the rifled tube.
3. At supercritical pressures, the HTC increased with enthalpy until it reached a maximum. After the maximum HTC, the HTC decreased as the bulk enthalpy increased. The increase in HTC resulted from the variation in the thermophysical properties. The influence of heat flux is related to the type of test section. The influence of heat flux on the heat-transfer characteristics in the smooth tube was mainly reflected in the pseudo critical region and the high-enthalpy region, where the HTC decreased as heat flux increased. The influence of the heat flux on heat-transfer characteristics in the rifled tube was mainly reflected in the low-enthalpy region, where the HTC increased with heat flux.
4. The heat transfer correlations of the smooth tube and rifled tube were fitted by the experimental data. The heat transfer correlations were divided by subcritical, near-critical, and supercritical pressure. The average relative errors are limited to 20%. All the correlations apply only to the specific tube type used in the experiments.
5. The friction resistance coefficient correlations of the smooth tube and rifled tube were fitted by the experimental data, and they were divided by subcritical/near-critical and supercritical pressure. The average relative errors were limited to 20%. All the correlations applied only to the specific tube type used in the experiments.

Author Contributions: Writing—review and editing, X.D.; Methodology, W.L.; Resources, X.Z.; Project administration, J.C.; Software, T.C.; Funding acquisition, D.Y. All authors have read and agreed to the published version of the manuscript.

Funding: This work is financially supported by the National Natural Science Foundation of China (No. 52076172).

Data Availability Statement: The data presented in this study are available on request.

Conflicts of Interest: The authors declare no conflict of interest.

Nomenclature

C_p	Specific heat, J/(kg·K)
d_i	Inner diameter, m
d_o	Outer diameter, m
E	Voltage, V
I	Current, A
G	Mass flux, kg/(m^2·s)
h_w	Specific enthalpy of fluid at the inner wall, J/kg

h_{in}	Inlet specific enthalpy of bulk fluid, J/kg
h_{out}	Outlet specific enthalpy of bulk fluid, J/kg
h_l	Single-phase heat transfer coefficient for the entire fluid as liquid, W/(m^2·K)
h_{tp}	Two-phase heat transfer coefficient, W/(m^2·K)
ΔH	Added enthalpy, J/s
λ_w	Thermal conductivity of test section, W/(m·K)
λ_g	Thermal conductivity of gas phase, W/(m·K)
P	Pressure, Pa
P_{cr}	Critical pressure, Pa
q	Heat flux, W/m^2
Q_E	Electric power, W
t_f	Bulk fluid temperature, °C
t_{iw}	Inner wall temperature, °C
t_{ow}	Outer wall temperature, °C
v_f	Specific volume while the characteristic temperature is the bulk fluid temperature
v_w	Specific volume while the characteristic temperature is the inner wall temperature
x	Dryness, kg/kg
η	Thermal efficiency of electric power, %
μ_g	Dynamic viscosity of gas phase, N·S/m^2
μ_l	Dynamic viscosity of liquid phase, N·S/m^2
ρ_g	Density of gas phase, kg/m^3
ρ_l	Density of liquid phase, kg/m^3
X_{tt}	Martinelli parameter
Subscript	
gw	Physical property of gas phase state water when the qualitative temperature is the inner wall
lo	Entire liquid phase state
l	Liquid phase state
g	Gas phase state
cr	Critical pressure
max	Maximum value for operating parameter in experiments
sl	Saturated liquid water
sv	Saturated vapor

References

1. Lei, X.L.; Li, H.X.; Zhang, W.Q.; Dinh, N.T.; Guo, Y.M.; Yu, S.Q. Experimental study on the difference of heat transfer characteristics between vertical and horizontal flows of supercritical pressure water. *Appl. Therm. Eng.* **2017**, *113*, 609–620. [CrossRef]
2. Yu, S.Q.; Li, H.X.; Lei, X.L.; Feng, Y.C.; Zhang, Y.F.; He, H.; Wang, T. Influence of buoyancy on heat transfer to water flowing in horizontal tubes under supercritical pressure. *Appl. Therm. Eng.* **2013**, *59*, 380–388. [CrossRef]
3. Wang, H.; Bi, Q.C.; Yang, Z.D.; Gang, W.; Hu, R. Experimental investigation on heat transfer characteristics of high pressures water in a vertical upward annular channel. *Exp. Therm. Fluid Sci.* **2013**, *45*, 169–179. [CrossRef]
4. Shen, Z.; Yang, D.; Chen, G.M.; Xiao, F. Experimental investigation on heat transfer characteristics of smooth tube with downward flow. *Int. J. Heat Mass Transf.* **2014**, *68*, 669–676. [CrossRef]
5. Swenson, H.S.; Carver, J.R.; Kakarala, C.R. Heat transfer to supercritical water in smooth bore tubes. *J. Heat Transf.* **1965**, *84*, 477–484. [CrossRef]
6. Vikhrev, Y.V.; Barulin, Y.D.; Konkov, A.S. A study of heat transfer in vertical tubes at supercritical pressures. *Teploenergetika* **1967**, *14*, 116–119.
7. Yamagata, K.; Yoshida, S.; Fujii, T.; Hasegawa, S.; Nishikaw, K. Forced convective heat transfer to supercritical water flowing in tubes. *Int. J. Heat Mass Transf.* **1972**, *15*, 2575–2593. [CrossRef]
8. Kolher, W.; Kastner, W. Heat transfer and pressure loss on rifled tubes. In Proceedings of the 8th International Heat Transfer Conference, San Francisco, CA, USA, 17–22 August 1986; Volume 5, pp. 2861–2964.
9. Kafenguaz, N.L.; Fedorov, M.I. Pseudoboiling and heat transfer in a turbulent flow. *J. Eng. Phys.* **1968**, *14*, 489–490. [CrossRef]
10. Grabezhnaya, V.A.; Kirillov, P.L. Heat transfer in pipes and rod bundles during flow of supercritical pressure water. *At. Energy* **2004**, *96*, 358–364. [CrossRef]
11. Yoshida, S.; Mori, H. Heat transfer to supercritical pressure fluids flowing in tubes. In Proceedings of the 1st International Symposium on Supercritical Water-Cooled Reatcor Design and Technology (SCR-2000), Tokyo, Japan, 6–8 November 2000. Paper No. 106. [CrossRef]

12. Mokry, S.; Pioro, I.; Farah, A.; King, K.; Gupta, S.; Peiman, W.; Kirillov, P. Development of supercritical water heat transfer correlation for vertical bare tubes. *Nucl. Eng. Des.* **2011**, *241*, 1126–1136. [CrossRef]
13. Wang, S.Y.; Yang, D.; Zhao, Y.J.; Qu, M.F. Heat transfer characteristics of spiral water wall tube in a 1000 MW ultra-supercritical boiler with wide operating load mode. *Appl. Therm. Eng.* **2018**, *130*, 501–514. [CrossRef]
14. Wang, S.Y.; Xin, Y.F.; Yang, D.; Dong, L.; Zhou, X.H. Experimental and numerical study on the heat transfer to supercritical water in an inclined smooth tube. *Int. J. Therm. Sci.* **2021**, *170*, 10711. [CrossRef]
15. Shen, Z.; Yang, D.; Li, Y.D.; Liang, Z.Y.; Wan, L. Numerical analysis of heat transfer to water flowing in rifled tube at supercritical pressures. *Appl. Therm. Eng.* **2018**, *133*, 704–712. [CrossRef]
16. Pioro, I.L.; Khartabi, H.F.; Duffey, R.B. Heat transfer to supercritical fluids flowing in channels-empirical correlations (Survey). *Nucl. Eng. Des.* **2004**, *230*, 69–91. [CrossRef]
17. Chen, J.C. Correlation for boiling heat transfer to saturated fluids in convective flow. *Ind. Eng. Chem. Process Dev.* **1996**, *5*, 322–329. [CrossRef]
18. Polyakov, A.F. Heat transfer under supercritical pressures. *Adv. Heat Transf.* **1991**, *21*, 1–51. [CrossRef]